Association of tamoxifen resistance and lipid reprogramming in breast cancer.

Susanne Hultsch[1*], Matti Kankainen[1], Lassi Paavolainen[1], Ruusu-Maaria Kovanen[1], Elina Ikonen[2], Sara Kangaspeska[1,3], Vilja Pietiäinen[1], and Olli Kallioniemi[1,4]

1. Institute for Molecular Medicine Finland, FIMM, Helsinki Institute for Life Sciences (HiLIFE), University of Helsinki, Helsinki, Finland,
2. Department of Anatomy, Faculty of Medicine, University of Helsinki, Helsinki, Finland,
3. Present affiliation: Helsinki Innovation Services (HIS)
4. Department of Oncology and Pathology, Karolinska Institutet and the Science for Life Laboratory (SciLifeLab), Stockholm, Sweden

Abstract

Background

Tamoxifen treatment of estrogen receptor (ER)-positive breast cancer reduces mortality by 31%. However, over half of advanced ER-positive breast cancers are intrinsically resistant to tamoxifen and about 40% will acquire the resistance during the treatment.

Methods

In order to explore mechanisms underlying endocrine therapy resistance in breast cancer and to identify new therapeutic opportunities, we created tamoxifen-resistant breast cancer cell lines that represent the luminal A or the luminal B. Gene expression patterns revealed by RNA-sequencing in seven tamoxifen-resistant variants were compared with their isogenic parental cells. We further examined those transcriptomic alterations in a publicly available patient cohort.

Results

We show that tamoxifen resistance cannot simply be explained by altered expression of individual genes, common mechanism across all resistant variants, or the appearance of new fusion genes. Instead, the resistant cell lines shared altered gene expression patterns associated with cell cycle, protein modification and metabolism, especially with the cholesterol pathway. In the tamoxifen-resistant T-47D cell variants we observed a striking increase of neutral lipids in lipid droplets as well as an accumulation of free cholesterol in the lysosomes. Tamoxifen-resistant cells were also less prone to lysosomal membrane permeabilization (LMP) and not vulnerable to compounds targeting the lipid metabolism. However, the cells were sensitive to disulfiram, LCS-1, and dasatinib.

Conclusion

Altogether, our findings highlight a major role of LMP prevention in tamoxifen resistance, and suggest novel drug vulnerabilities associated with this phenotype.

Keywords

Tamoxifen resistance; breast cancer; lysosomal membrane permeabilization; RNA-sequencing; drug sensitivity and resistance testing

Background

Approximately two thirds of breast cancers are estrogen receptor (ER) positive. As the receptor stimulates proliferation of mammary epithelial cells, it is also an important target in anti-hormonal cancer therapy. One of the most prescribed ER antagonists for first line therapy is tamoxifen that has helped millions of women since its discovery 50 years ago [1]. However, *de novo* or acquired drug resistance towards tamoxifen is a notable problem and the later affects approximately 40% of patients receiving tamoxifen [2].

In addition to its intended anti-cancer effects, tamoxifen is known to have both direct and indirect effects on the cellular lipid metabolism. It has been shown to reduce blood cholesterol levels [3] and to be protective against cardiovascular diseases [4]. However, approximately 43% of the patients treated with tamoxifen develop hepatic steatosis, including the accumulation of neutral lipids to lipid droplets in hepatic cells [5]. Tamoxifen can regulate the lipid balance e.g by binding to the microsomal antiestrogen binding sites (AEBS), which are associated with cholesterol metabolism [6]. This mechanism has been linked to control cell growth, differentiation and apoptosis in the presence of reactive oxygen species (ROS) and has been established as another mode by which tamoxifen induces cytotoxicity [7,8].

On the other hand, reprogrammed metabolism is one hallmark of cancer cells [9] and has recently been suggested as a new mode of drug resistance in cancer therapy [10,11]. The metabolic intermediates can supply cancer cells with membrane phospholipids, with energy through the β-oxidation pathway or with pro-tumorigenic lipid-signaling molecules such as lysophosphatidic acid [12]. Some studies even suggested a role of cholesterol metabolism in tamoxifen resistance [13] and Borgquist et al. showed an improved clinical outcome for ER-positive breast cancer patients receiving cholesterol-lowering medication during their adjuvant endocrine therapy [14].

In the present study, we have delineated mechanisms underlying tamoxifen resistance by extending our drug screening and exome sequencing analyses on tamoxifen-resistant cell lines [15] by performing RNA-sequencing on the tamoxifen-resistant and their isogenic, tamoxifen-sensitive parental cell lines, and searched for genes and pathways that may be involved in the acquired resistance. Differential gene expression and pathway analysis confirmed that endocrine resistance is not triggered by one common mechanism but involves several functional pathways, depending on the cell type [15]. Through the integration with public data [16], the usefulness of our breast cancer cell line model was assessed and the relevance of the identified transcriptomic alterations verified in this patient cohort. By focusing on the isogenic T-47D cell variants, we showed that genes in the cholesterol pathway were differentially expressed between tamoxifen-sensitive and tamoxifen-resistant cells. These results were supported by a striking accumulation of lysosomal cholesterol upon tamoxifen treatment, increased neutral lipid amounts after the development of resistance. Markedly, tamoxifen treated cells were also found to be less prone to lysosomal membrane permeabilization, suggesting that altered lysosomal integrity may confer resistance to tamoxifen. Finally, using high-content phenotypic drug sensitivity profiling of 33 drugs targeting lipid metabolism as well as inducing lysosomal membrane leakage, we identified drug candidates for overwriting the tamoxifen resistance and potentially being beneficial for breast cancer patients unresponsive to tamoxifen.

Methods

Cell culture

The development, characterization and culturing of the tamoxifen-resistant and their isogenic parental cell lines has been published previously [15]. If not otherwise stated, the parental cell lines (luminal A: MCF-7, T-47D, ZR-75-1, luminal B: BT-474) [17] were cultured without tamoxifen and the tamoxifen-resistant cell lines, marked with Tam throughout this study (MCF-7 Tam1, T-47D Tam1 & Tam2, ZR-75-1 Tam1 & Tam2, BT-474 Tam1 & Tam2) were supplemented with 1 µM 4-OH-tamoxifen (Sigma).

RNA-sequencing and data analysis of cell line data

RNA isolation, library preparation, sequencing, and data-analysis were done as explained in Kumar A et al. [18]. Briefly, total RNA was isolated using miRNeasy kit (Qiagen) and its quality was controlled by using the Agilent Bioanalyzer with the RNApico chip (Agilent). Qubit RNA-kit (Life Technologies) was used to quantitate RNA amount per sample. The strand-specific paired-end RNA-sequencing library was prepared then with ScriptSeq™ Complete kit for human/mouse/rat (Illumina). The library preparation included the ribodepletion of rRNA from 1 µm of total RNA and generation of double stranded cDNA by revers transcription with random hexamers for generation of cDNA. SPRI beads (Agencourt AMPure XP) were used to purify the libraries and to remove fragments less than 200 bp in length. The mean fragment size ranged from 300 to 400 nucleotides. The library quality was evaluated on the High Sensitivity chip by Agilent Bioanalyzer (Agilent). The paired-end sequencing was performed using the Illumina HiSeq 2000 (Illumina) instrument according to the manufacturer's instructions.

RNA-sequencing data analysis was performed as described in detail in Kumar et al. [18] and included pre-processing of read data, gap-aware alignment of the read data to the human reference genome (Ensembl GRCh38) with the guidance of the EnsEMBL reference gene models (EnsEMBL v80), read summarization against EnsEMBL v80 gene features, and identification of fusion genes. Fusion genes were detected using FusionCatcher, which was applied to raw, un-processed read files with default parameters [19]. The raw and processed sequencing data have been deposited in the GEO database [GEO: GSE111151].

Integration of public and cell-line transcriptomic data and differential expression analysis

Public patient transcriptome data [16] was downloaded from GEO database [20] and analyzed as cell line sequencing data, but using the EnsEMBL v82 gene features in all steps. Alignment files were combined with alignment files from the cell-line samples and count estimates were generated against EnsEMBL v82 gene features using subreadR [21]. Count data was then assigned to EnsEMBL information using biomaRt [22], normalized using the trimmed mean of M-values (TMM) method [23], converted to CPM (counts per million) estimates using edgeR [24], corrected for the batch effect associated with the study origin using limma [25], and filtered for lowly expressed features showing log2 expression ≤ 1 in over half of samples. Default parameters were used. In the lack of biological replicates, differentially expressed genes were identified as those with a log2 ratio of >= |1| and CPM difference of >= |10| against its matched parental cell line. Further, we used Enricher [26,27] with the list of differentially expressed genes to determine pathways that were involved in the development of tamoxifen resistance for each parental vs. resistant cell line comparison. Pathways with an adjusted p-value less than 0.001 (1E-3) were accepted as significantly altered. Log2 ratios of differentially expressed genes of the cell lines were visualized using heat maps. In the heat map analysis, genes and samples were ordered using unsupervised complete linkage clustering with Euclidean distance measure [15]. Patient and cell line data was visualized using principle component analysis and heat maps as described above using biomaRt to extract cholesterol genes under the reactome.ID R-HSA-191273.

122 **Measurement of triglycerides and cholesterol esters**

123 Parental and resistant T-47D cells were plated on 6-well plates and grown in their default media +/- 1 µM
124 4-OH-tamoxifen for 72 h in triplicates. Cells were scraped in 0.2 N NaOH for lipids extraction as previously
125 described [28]. Cell lysates were also examined for protein amount. Free cholesterol, cholesterol esters
126 and triglycerides were resolved on TLC plates using hexane/diethyl ether/acetic acid (80:20:1) as the
127 mobile phase prior to the visualization of lipids by charring. The lipid bands were quantified by ImageJ [29]
128 from scanned plates and the lipid amounts were determined based on the standard curves for
129 triglycerides, cholesterol esters and free cholesterol.

130 **Immunofluorescence staining and Western blotting**

131 Parental and resistant T-47D cells were seeded on coverslips and grown in the default media +/- tamoxifen
132 for 72 h. Cells were fixed with 4 % paraformaldehyde for 20 minutes at room temperature, and
133 permeabilized with 0.3 % Triton X-100 for 5 minutes, followed by 30 min blocking with 3 % BSA-PBS at
134 37 °C. The primary and secondary antibodies were diluted in 1 % BSA-PBS and consecutively incubated for
135 60 and 30 min at 37 °C. For detection of free cholesterol, cells were stained with 0.05 % filipin (Sigma) in
136 10 % FBS–PBS blocking solution for 30 minutes at 37 °C. Antibodies were prepared in 5 % FBS-PBS and
137 incubated as described above. Nuclei were stained with DRAQ5 (Biostatus). For detecting lipid droplets,
138 LipidTOXGreen neutral lipid stain (ThermoFisher Scientific) was diluted 1:200 in PBS to stain freshly fixed
139 coverslips following the manufactures protocol and detecting the nuclei with Hoechst. Stained coverslips
140 were mounted with Prolong Gold anti-fade reagent (Invitrogen) and imaged with a Nikon 90i microscope
141 (Nikon). For Western blotting, cells were grown on 10 cm dishes, and lysed in Laemmli buffer.
142 Immunoblotting was performed as previously described [30] using the Odyssey Blocking Buffer (Licor) for
143 blocking and the antibody dilutions. Information about the antibodies and their dilution used for
144 immunofluorescence as well as Western blotting is available at Additional File 1.
145

146 **Lysosomal membrane permeabilization (LMP) assay**

147 In order to measure the integrity of lysosomal membranes, we performed the detection of damaged
148 lysosomes by galectin-1 and -3 translocation according to the previously published protocol [31]. We first
149 established that galectin-3 was in our cell lines a more reliable marker to detect its translocalization to the
150 lysosomes compared to galectin-1. We then seeded 2000 cells/well of T-47D, T-47D Tam1 and Tam2 on
151 PE Cell-Carrier 384-well plate +/- 1 µM 4-OH-tamoxifen. After 72 h incubation, 1 mM LLMOe was added
152 as LMP induction control and incubated for 1 h. Cells were then fixed with 4 % PFA and stained with
153 galectin-3 detected with Alexa 568 (461nm), ceruloplasmin as cell segmentation marker detected with
154 Alexa 488 (488 nm, Additional file1) and Hoechst (405nm) for detection of the nuclei. 16 fields-of-view
155 were acquired with the two sCMOS cameras (2160x2160 pixels) containing Opera Phenix HCS system
156 (PerkinElmer) in a widefield mode with the 40x water immersion objective (NA 1.1). Exposure time and
157 laser power were kept constant for each individual staining across different cell lines and conditions. We
158 utilized the Columbus Image Data Storage and Analysis System (PerkinElmer) to analyze the multi-channel
159 images. First, the images were preprocessed to correct non-uniform illumination. Next, individual nuclei
160 were segmented from the Hoechst channel. The minimum area of a nucleus was set to 30 μm^2 to remove
161 the detection of debris in the image background. Starting from the detected nuclei, the segmented regions
162 were propagated to cover cell cytoplasm stained with ceruloplasmin. The cells that touched the image
163 border were discarded. Finally, spot detection was used to segment galectin-3 stained spots. The
164 maximum radius of the spots was set to 1 µm. We defined cells with more than 1 spot as galectin-3 positive

to exclude false positive detection. Further, we calculated the percentage of galectin-3 positive cells and the average spots per cell.

Drug sensitivity and resistance testing (DSRT) and high-content phenotypic drug profiling

33 compounds that target lipid and cholesterol metabolism, or induce LMP, were selected for the DSRT by literature and vendor research (Additional file 2). As in the previous DSRT screens [15,32], the dissolved drugs were transferred in five different concentrations covering a 10 000-fold concentration range into 384-well plates in duplicates mirrored after column 12. 1500 cells of T-47D parental, Tam1, and Tam2 cells were then seeded into the wells in normal growth media on columns 1-12 of each plate and in media supplemented with 1 µM 4-OH-tamoxifen on columns 13-24. The cells were then incubated for 72 h at 37 °C and cell viability was measured by CellTiter-Glo (CTG) Cell Viability Assay (Promega) with the PHERAstar plate reader. Data was normalized to negative (DMSO only) as well as positive (100 µmol/l benzethonium chloride) controls, logistic dose response curves fitted using the Marquardt-Levenberg algorithm, and Drug Sensitivity Score (DSS) calculated as described previously [33], and implemented in the in-house bioinformatics analysis pipeline Breeze.
For the high-content phenotypic drug profiling, plates were fixed with 4 % PFA-PBS after incubation with drugs for 72 h, and stained with LipidTOXGreen neutral lipid stain (ThermoFisher Scientific) diluted 1:200 in PBS and Hoechst for nuclei detection. 25 fields-of-view per well were acquired with the PE Opera Phenix HCS system (PerkinElmer) in a confocal mode with the 40x water immersion objective (NA 1.1). Exposure time and laser power were kept constant for each individual staining across different cell lines and conditions. Images were analyzed using a custom pipeline to measure LipidTOXGreen signal and image-based DSS based on cell counts. Images were preprocessed by applying flatfield correction using CIDRE method [34], and then stitching corrected 25 fields-of-view images to a single image of a well for each channel. The stitching was done to enable the analysis of cells crossing internal borders of images. The stitching produced images of approximately 10400^2 pixels in size which were resampled to 5200^2 pixels to reduce computational capacity needed for image analysis. Images were analyzed with CellProfiler 2.2.0 [35]. First, nuclei were segmented from the Hoechst channel using Otsu thresholding followed by separation of touching nuclei with watershed transform on distance transformed image. LipidTOXGreen channel was segmented using adaptive Otsu thresholding and propagation outwards from individual nuclei. The LipidTOXGreen signal was measured in segmented regions for each individual cell. Logistic dose response curves were fitted to cell counts to calculate image-based DSS in Breeze.

Statistical analysis

For all experiment that were at least done in triplicates the values were expressed as mean ± SD. One way ANOVA was performed on the mean of each measurement followed by Tukey test to enable multiple comparisons between groups. Statistically significance was accepted as $p<0.05$. All comparisons of the measurement of triglycerides, free cholesterol and cholesterol esters, LMP assay, and LipidToxGreen staining can be found in Additional file 3.

Results

Each tamoxifen-resistant cell line develops its individual gene expression and fusion gene profile

RNA-sequencing was performed to detect differentially expressed genes and pathways between parental and resistant cell lines. Between 85 and 181 million filtered reads were obtained per sample (Additional file 4), providing means to obtain expression estimates between 33,600 and 37,000 genes per sample. We determined differential gene expression as log2 change of >|1|, and the difference of gene expression >

207 |10| CPM between the resistant clone and its isogenic parental cell line (see Methods). Using this filtering,
208 we identified >1200 differentially expressed genes in MCF-7- and T-47D-derived cells, and <400 genes in
209 BT-474- and ZR-75-1-derived cells. On average 59 % of differentially expressed genes were upregulated in
210 the majority of resistant cell lines (Table 1). Interestingly, only about 35 % of altered genes in T-47D as
211 well as BT-474, and only 24 % in ZR-75-1 were shared between the resistant cells derived from the same
212 parental cell line (Additional figure 1A). Additionally, no common differentially expressed genes were
213 identified, highlighting that each of the cell lines had developed resistance through a distinct molecular
214 pattern (Figure 1A and B). Nevertheless, common genes (*SERPINA1, PLXDC2, NAV1*, *DOCK10* and *LRP1*)
215 with altered expression were detected in the luminal A cell lines (Additional figure 1B). No shared fusion
216 genes across the cell lines were detected apart from the read-through fusions *ABCC11-ABCC12* and
217 *TRIM3-HPX* (Additional file 5).

218 **Tamoxifen-resistant cell lines resemble tamoxifen-treated patient cases**

219 To compare the tamoxifen-resistant cell line models with breast cancer patient samples, we reanalyzed
220 the McBryan et al. RNA-sequencing data [16]. Following the analysis with our RNA-sequencing pipeline
221 and correction for batches (patient samples and cell lines), we determined differentially expressed genes
222 between primary and metastatic tumors and integrated the data with the transcriptome data from our
223 cell lines. The results were in line with McBryan's et al., and indicated that only about 2.5 % of differentially
224 expressed genes were shared between all the patients (Figure1 C). Interestingly, we found that patient-
225 specific expression profiles clustered together with the expression of the luminal A cells (Figure 1D).
226 Furthermore, *SERPINA1*, which was differentially expressed in the tamoxifen-resistant luminal A cell lines
227 (being upregulated in MCF-7 Tam1 and downregulated in T-47D Tam1, T-47D Tam2, ZR-75-1 Tam1 and
228 ZR-75-1 Tam2), also changed its expression in the patient samples (being up-regulated in all three
229 metastatic tumors). *CP* (Ceruloplasmin), a gene that was highly upregulated in the resistant T-47D cell
230 lines (240-290 fold-increase) as well as MCF-7 Tam1 (26 fold-increase), was also found to be
231 overexpressed in all the 3 metastatic patient samples ranging from 12-fold increase (patient 2) to 50-57
232 fold increase (patient 1 and 3, respectively, Additional file 6).

233 **Triglycerides and cholesterol esters are increased in the resistant T-47D cell lines**

234 To reveal pathways associated with tamoxifen resistance, we analyzed the differentially expressed genes
235 with Enrichr [26,27]. Based on Enrichr's Reactome 2016 analysis with an adjusted p-value below 0.001,
236 we observed multiple enriched pathways in different resistant cell lines (Table 2 and Additional File 7).
237 The most striking differences were found in the T-47D Tam1 and Tam2 cells, which displayed changes in
238 metabolism associated genes, especially those involved in cholesterol and related lipid metabolism (Table
239 2, Figure 2A).

240 In addition, we observed an upregulation of genes involved in cholesterol biosynthesis in all three
241 metastatic patient samples from McBryan et al. study (Figure 2A). Therefore, we focused our studies on
242 these pathways within the T-47D cell lines (Table 2 and Additional File 7). To investigate whether
243 deregulation of genes involved in cholesterol biosynthesis could affect the cellular cholesterol balance,
244 we stained cellular free cholesterol with filipin, a fluorescent cholesterol-binding compound. Notably, we
245 observed increased intracellular amounts of free cholesterol in the resistant cells, displaying a cumulus
246 cloud-like staining pattern (Figure 2B). To quantify the presence of major cellular lipid species e.g.
247 cholesterol, cholesterol esters, and triglycerides, their amounts were further determined with thin layer
248 chromatography. The total cellular free cholesterol remained unchanged, suggesting that only the

249 distribution of free cholesterol was altered in the resistant cells. However, we observed an increase in
250 neutral lipids (cholesterol esters and triglycerides) upon tamoxifen treatment. The increase in triglycerides
251 was significantly high (4 to 7 fold-increase) in resistant cells compared to parental cells (Figure 2C). To
252 visualize the changes in neutral lipid amounts as well as their intracellular distribution, we stained the
253 cells with LipidToxGreen, a fluorescent dye binding specifically to neutral lipids. The analysis indicated that
254 most of the neutral lipids accumulated in enlarged lipid droplets, which fill the cytoplasm (Figure 2D).
255 Moreover, RNA sequencing results implicated that the expression of Peroxisome Proliferator-Activated
256 Receptor gamma (*PPARG*), which is known to regulate several lipid droplet proteins, was upregulated in
257 resistant cells. In addition, the ATP Binding Cassette Subfamily A Member 1 (*ABCA1*), which functions as a
258 cholesterol efflux pump was downregulated (Additional file 6).

259 **Tamoxifen-resistant cells show altered morphology of lysosomes, have altered processing of Cathepsin**
260 **D, and are less susceptible to lysosomal membrane permeabilization**

261 To localize the accumulated free cholesterol, we co-stained free cholesterol (filipin) with antibodies
262 detecting the lysosomal-associated-membrane-proteins 1 and 2 (Lamp1 and Lamp2). Based on this
263 analysis, we observed that most of the free cholesterol accumulated into lysosomes. We also discovered
264 an increase in the amount and size of lysosomes as well as divergences in shape compared to their typical
265 round form seen in the parental cell lines (Figure 3A & B). As the tamoxifen-resistant cells displayed a
266 prominent phenotype with free cholesterol accumulation to structurally disturbed lysosomes, we studied
267 the amounts of cathepsin D and its lysosomal maturation. Cathepsins are lysosomal proteins that help to
268 maintain the homeostasis of cell metabolism and are involved in apoptotic signaling as well as in lysosomal
269 membrane permeabilization. Furthermore, the expression of cathepsin D is known to be regulated by
270 estrogen [36]. As expected, we observed a decrease of mature cathepsin D (28 kDa) under tamoxifen
271 treatment in parental and resistant cell lines, suggesting that tamoxifen can regulate the expression
272 and/or processing of cathepsin D [37]. Whilst addition of tamoxifen also caused an upregulation of the
273 precursors of cathepsin D in the parental cell line, such an increase was not obvious in the resistant cell
274 lines (Figure 3E), suggesting that the maturation of cathepsin D in the lysosomes may be affected.

275 As lysosomal integrity, with cholesterol content of lysosomal membranes and cathepsin D among its
276 regulators, plays an important role in the induction of cell death [38], we monitored the translocation of
277 galectin-3 to detect LMP. Given that galectin-3 translocation to the lysosomes was not detected in the
278 parental cells when grown without tamoxifen, and that only very few tamoxifen-treated cells showed
279 galectin-3 spots (Figure 3C & D), lysosomes were most likely undamaged and functional in all cells. Further,
280 by inducing LMP with 1 mM LLOMe we were able to observe that tamoxifen treated resistant cells were
281 less susceptible to LMP compared to the parental cell line, having only 51-53% of cells with galectin-3
282 spots under tamoxifen treatment and significantly less galectin-3 spots per cell (Figure 3C & D). This
283 suggests that circumvention of LMP in the resistant cells leads not only to tamoxifen resistance but may
284 also decrease their sensitivity to other drugs.

285 **Drug testing of tamoxifen resistant cells reveals sensitivity to dasatinib, disulfiram and LCS-1**

286 Guided by our RNA-sequencing results we selected 33 drugs, known to affect the genes or pathways
287 involved in lysosomal alterations and lipid metabolism as well as some drugs identified in our previous
288 screen (Additional file 2, [15]). As readouts for the DSRT, we applied both enzymatic cell viability
289 measurement (CTG) as well as a phenotypic image-based analysis using LipidToxGreen to observe neutral
290 lipids in lipid droplets together with Hoechst to detect nuclei.

291 The cell viability measurement revealed drugs that reduced ATP levels in tamoxifen-resistant cells similarly
292 to the control cells, independently of their lipid accumulation phenotype (Figure 4A, Additional file 8).
293 Dasatinib, a dual Abl/Src inhibitor was more effective in killing the tamoxifen resistant cell lines compared
294 with the parental cells in agreement with our previous results [15]. Tamoxifen-resistant cells were more
295 sensitive to microtubule depolymerizing drugs, such as vincristine and vinorelbine, when measured by
296 ATP amounts. Interestingly, the T-47D Tam2 cells were especially sensitive to vinorelbine induced
297 cytotoxicity (Figure 4A, Additional file 8). The mitotic inhibitors paclitaxel and docetaxel (microtubule
298 stabilizers) were less effective in the T-47D Tam1 cells. (Figure 4A, Additional file 8).
299 The most effective drug against all the T-47D clones was disulfiram, a specific inhibitor of aldehyde-
300 dehydrogenase (ALDH1). All the clones responded to AZD8055, a dual mTOR inhibitor, although T-47D
301 Tam1 and Tam2 showed reduced sensitivity. Atorvastatin, which inhibits HMGCoA reductase, did not
302 affect the CTG DSS levels (Figure 4A) but was able to reduce the cell count in the parental and even more
303 in the T-47D Tam2 cells (Figure 4B). The SOD-1 inhibitor LCS-1 was effectively killing both parental and
304 resistant T-47D clones, and RSL-3, a ferroptosis activator due to inhibition of glutathione peroxidase 4,
305 induced cell death in all the cell lines, with somewhat reduced response in T-47D Tam1 (Figure 4B,
306 Additional file 8).
307 To see whether any of the compounds are able to revert the lipid phenotype prior to reducing the cell
308 viability (ATP-measurement) or induction of cell death (cell count), we specifically monitored the changes
309 in neutral lipids by quantifying the average LipidToxGreen intensity per well (Additional file7). The
310 measured significant increase in the intensity was within the 2-fold range, and we were able to confirm
311 the trends from the biochemical screen where we observed a neutral lipid accumulation in the resistant
312 cell lines (Figure 2C, Figure 4C). Whereas most of the drugs had minor effects on the LipidToxGreen
313 intensity (Additional file 9), the LXR-agonist TO901317 increased the lipid phenotype most strikingly in the
314 parental cells, with less increase particularly in T-47D Tam1 cells (Figure 4D). In addition, methyl-β-
315 cyclodextrin, a membrane cholesterol-depleting agent, caused a lipid droplet accumulation phenotype,
316 mostly in the parental cell line prior to cell killing in the highest concentration (Additional file 9).
317
318 **Discussion**

319 In this study, we utilized RNA-sequencing and pathway analysis to understand the underlying tamoxifen
320 resistance and identify resistance-specific drug vulnerabilities. We revealed the involvement of lipid
321 metabolism in tamoxifen resistance as well as pointed out potential therapeutic ways to target these
322 pathways.

323 Gene expression analysis on tamoxifen-resistant cells reinforced our previous finding on breast cancer
324 cells using a variety of molecular pathways as they acquire tamoxifen resistance [15]. The difference in
325 gene expression was reflected in the scale and scope of differentially expressed genes, and in the lack of
326 shared genes across all the cell lines (Figure 1). In agreement with this finding, the only study that has
327 performed sequential tumor transcriptome analysis on patients developing endocrine resistance, also
328 identified less than 3% of differentially expressed genes across patients (Figure 1C [16]). Despite the
329 overall transcriptome profiles being distinct across the resistant cell lines, we were able to identify five
330 genes that were concordantly differentially expressed in the luminal A subtype resistant cells (Additional
331 figure 1B). Of these, *SERPINA1,* encoding for a serine protease inhibitor primarily targeting elastase, is
332 known to bind ER in a 17β-estradiol (E2) - independent manner, which leads to an increase in its
333 expression [39]. Therefore the observed expression changes could be due to the down- and upregulation

334 of ER in these cell lines [15]. Interestingly, in all three metastatic samples from the McBryan *et al.* study,
335 we observed an increase in *SERPINA1*, which is accompanied by a slight increase of *ESR1* transcription
336 (Additional file 6). Pathway analysis of the differentially expressed genes identified several paths involved
337 in acquired tamoxifen resistance (Table 2, Figure 2A).

338 In this study, we investigated the tamoxifen-induced changes observed in lipid metabolism, which
339 occurred in the T-47D tamoxifen-resistant cell lines (Table 2, Figure 2). We also made the equivalent
340 finding in a patient's metastatic tissue (Figure 2A). As the metastasis was found in the liver [16], the
341 observed lipid metabolism pathway profiles have to be interpreted with caution. Nevertheless, our
342 findings suggest that the lipid phenotypes could already develop in the breast cancer cells [40] and is not
343 solely induced by the liver environment.

344 Further, our studies with the T-47D tamoxifen-resistant cell lines show an increase of free cholesterol into
345 strikingly enlarged lysosomes (Figure 2B, Figure 3A & B, [41]). It has been shown that accumulation of
346 cholesterol, an increase in Lamp1 and Lamp2 as well as downregulation of cathepsins prevents lysosomal
347 membrane permeabilization [42–45], a process which leads to different forms of cell death such as
348 apoptosis, necroptosis, necrosis and ferroptosis [38]. Indeed, our data on the resistant cells shows an
349 increase in cholesterol, Lamp1 and Lamp2, as well as a decrease in cathepsin D (Figure 2B, Figure 3A, B
350 and E [37]). A short-term tamoxifen treatment diminished directly the LLOMe-induced LMP. The T-47D
351 Tam1 and Tam2 were even more resistant towards LMP (Figure 3C and D), showing that tamoxifen can
352 hinder it, and in acquired resistance, this phenomenon is even more prominent. Thus, impeded lysosomal
353 membrane permeabilization may additionally enhance the co-resistance to other cancer drugs during
354 acquired tamoxifen resistance.

355 Reducing the reactive oxygen species (ROS) is another mechanism by which cells avoid lysosomal induced
356 cell death [44]. We speculate that resistant T-47D cells are able to reduce oxidative stress by upregulation
357 of *SOD1* (Additional file 6) and may therefore be less sensitive to lysosomal cell death. This hypothesis is
358 further supported by the fact that the resistant cells were highly sensitive to the SOD1 inhibitor LCS-1. The
359 capability of erastin to activate ferroptosis is instead inhibited by antioxidants, and it was more effective
360 in parental than in resistant cells. The ferroptosis activator RSL-3, which inhibits the glutathione
361 peroxidase 4, an enzyme that protects from oxygen damage, induced cell death in all the cell lines (Figure
362 4 and Additional file 8). This further supports the assumption that the T-47D cells are able to reduce
363 oxidative stress and are therefore less sensitive to lysosomal cell death.

364 Disulfiram, which targets ALDH1 to increase oxidative stress, was highly effective in both parental and
365 tamoxifen-resistant T-47D cell clones (Figure 4 and Additional file 8). The effectiveness of disulfiram is
366 currently investigated in metastatic breast cancer in a phase II clinical trial [46]. *ALDH2*, another target of
367 disulfiram, is upregulated in T-47D Tam1 but not in Tam2 (Additional file 6). High levels of ALDH1 have
368 been shown to predict resistance in women treated with tamoxifen [47], but as *ALDH1A1* is expressed at
369 very low levels in the T-47D cell lines (Additional file 6), we assume that the sensitivity to disulfiram could
370 be due to its capability to disable antioxidation mechanisms of the cells [48].

371 A significant increase in triglycerides, stored in large lipid droplets (LDs) was observed in tamoxifen-
372 resistant cells (Figure 2C, D and Figure 4C). Free fatty acids are enzymatically converted to triacylglycerol,
373 and then incorporated into LDs. Packaging of excess lipids into LDs could be seen as an adaptive response
374 to fulfilling energy supply without hindering mitochondrial or cellular redox status and keeping the
375 concentration of lipotoxic intermediates low [49]. Accordingly, high LDs and stored cholesterol esters in

376 tumors are considered as hallmarks of aggressive cancer [50]. LD-rich cancer cells have also been shown
377 to be more resistant to chemotherapy [51]. We found over 3-fold upregulation of stearoyl-CoA desaturase
378 (*SCD*), encoding for a rate-limiting enzyme in the biosynthesis of monounsaturated fatty acids, in the
379 tamoxifen-resistant T-47Ds (Additional file 6). Whether it alone is able to induce the increase in TGs,
380 remains to be investigated. In line with this speculation, *SCD* overexpression has been observed, in
381 different cell types as well as in tamoxifen-induced hepatocyte steatosis, to significantly increase the rate
382 of triglyceride synthesis [52]. The compounds directly affecting lipid metabolism, such as C75, Bezafibrate,
383 T 0070907, TO901317, and Orlistat, had no or only little effect on cell viability or the lipid phenotype
384 (Figure 4 and Additional files 8, 9). This suggests that the T-47D cells are able to compensate the drug-
385 induced lipid imbalance with several mechanisms, which would be compelling to study in depth.

386 **Conclusion**

387 Taken together, our results highlight that tamoxifen resistant cell lines can potentially be used as a
388 representative model for studies of tamoxifen-resistant patients. We propose that the breast cancer cells
389 can acquire tamoxifen resistance by dysregulation of different cellular pathways, dependent on their
390 individual molecular phenotypes. Here, we highlight the inhibition of lysosomal membrane
391 permeabilization as one of the mechanisms to avoid cell death, whereas an increase in neutral lipids may
392 enable the further survival of these cells. We further propose that drugs targeting cellular antioxidation
393 machinery may be able to overcome tamoxifen resistance. However, investigating the relevance of the
394 proposed mechanism of acquired resistance in patients remains a challenge. Given the vulnerability of
395 tamoxifen resistant cells to approved drugs such as disulfiram and dasatinib, it would be interesting to
396 investigate whether these compounds could also be effective in clinical trials in tamoxifen-resistant breast
397 cancer patients.

398 **List of abbreviations**

399 ER, estrogen receptor; DSRT, drug sensitivity and resistance testing; LMP, lysosomal membrane
400 permeabilization, ROS, reactive oxygen species

401 **Declarations**

402 **Acknowledgments**

403 We acknowledge Prof. Marja Jäättelä (Danish Cancer Society Research Institute, Denmark) for comments
404 to lysosomal membrane permeabilization assays. Anna Uro from the Ikonen laboratory (University of
405 Helsinki) is acknowledged for technical assistance in biochemical lipid determination. High Throughput
406 Biomedicine (HTB) unit (Laura Turunen, Maria Nurmi and Swapnil Podar), Sequencing unit (Pirkko Mattila),
407 and High Content image Analysis (HCA) unit at the Institute for Molecular Medicine Finland (FIMM), HiLIFE,
408 University of Helsinki, and Biocenter Finland are acknowledged of the high throughput drug profiling and
409 high content imaging expertise. Piia Mikkonen is acknowledged for technical help with the drug screens.

410 **Fundings**

411 Sigrid Juselius Foundation, TEKES FiDiPro Fellow Grant 40294/1, Academy of Finland Centers of Excellence
412 in Translational Cancer Biology and in Biomembrane Research, Biocentrum Helsinki grants are
413 acknowledged for the financial contributions to this study.

414 **Authors' contributions**

SH and VP designed the study. SH performed experiments, data analysis and wrote the manuscript. MK performed RNA-Seq analysis and contributed to writing the manuscript. LP analyzed the lipid screen and contributed to writing the manuscript. RMK performed the LMP experiment. EI provided resources for the biochemical assay and participated in editing the manuscript. SK provided resources for RNA-sequencing and participated in editing the manuscript. VP and OK supervised the project and participated in manuscript writing and editing. All authors read and approved the final manuscript.

Competing interests

The authors declare that they have no competing interests.

Availability of data and materials

All data generated or analyzed during this study are included in this published article and its additional files. The raw and processed sequencing data have been deposited in the GEO database [GEO: GSE111151].

Ethics approval and consent to participate

Not applicable.

Consent for publication

Not applicable.

References

1. Jordan VC. Tamoxifen: a most unlikely pioneering medicine. Nat Rev Drug Discov. 2003;2:205–13.

2. Ring A, Dowsett M. Mechanisms of tamoxifen resistance. Endocr Relat Cancer. 2004;11:643–58.

3. Caleffi M, Fentiman IS, Clark GM, Wang DY, Needham J, Clark K, et al. Effect of tamoxifen on oestrogen binding, lipid and lipoprotein concentrations and blood clotting parameters in premenopausal women with breast pain. J Endocrinol. 1988;119:335–9.

4. McDonald CC, Alexander FE, Whyte BW, Forrest AP, Stewart HJ. Cardiac and vascular morbidity in women receiving adjuvant tamoxifen for breast cancer in a randomised trial. The Scottish Cancer Trials Breast Group. BMJ. 1995;311:977–80.

5. Nishino M, Hayakawa K, Nakamura Y, Morimoto T, Mukaihara S. Effects of tamoxifen on hepatic fat content and the development of hepatic steatosis in patients with breast cancer: high frequency of involvement and rapid reversal after completion of tamoxifen therapy. AJR Am J Roentgenol. 2003;180:129–34.

6. Kedjouar B, de Médina P, Oulad-Abdelghani M, Payré B, Silvente-Poirot S, Favre G, et al. Molecular characterization of the microsomal tamoxifen binding site. J Biol Chem. 2004;279:34048–61.

7. Payré B, de Medina P, Boubekeur N, Mhamdi L, Bertrand-Michel J, Tercé F, et al. Microsomal antiestrogen-binding site ligands induce growth control and differentiation of human breast cancer cells through the modulation of cholesterol metabolism. Mol Cancer Ther. 2008;7:3707–18.

448 8. Bekele RT, Venkatraman G, Liu R-Z, Tang X, Mi S, Benesch MGK, et al. Oxidative stress contributes to
449 the tamoxifen-induced killing of breast cancer cells: implications for tamoxifen therapy and resistance.
450 Sci Rep [Internet]. 2016 [cited 2017 Aug 21];6. Available from:
451 http://www.ncbi.nlm.nih.gov/pmc/articles/PMC4756695/

452 9. Pavlova NN, Thompson CB. The Emerging Hallmarks of Cancer Metabolism. Cell Metab. 2016;23:27–
453 47.

454 10. Bacci M, Giannoni E, Fearns A, Ribas R, Gao Q, Taddei ML, et al. miR-155 Drives Metabolic
455 Reprogramming of ER+ Breast Cancer Cells Following Long-Term Estrogen Deprivation and Predicts
456 Clinical Response to Aromatase Inhibitors. Cancer Res. 2016;76:1615–26.

457 11. Chen C-L, Uthaya Kumar DB, Punj V, Xu J, Sher L, Tahara SM, et al. NANOG Metabolically Reprograms
458 Tumor-Initiating Stem-like Cells through Tumorigenic Changes in Oxidative Phosphorylation and Fatty
459 Acid Metabolism. Cell Metab. 2016;23:206–19.

460 12. Zaidi N, Lupien L, Kuemmerle NB, Kinlaw WB, Swinnen JV, Smans K. Lipogenesis and lipolysis: the
461 pathways exploited by the cancer cells to acquire fatty acids. Prog Lipid Res. 2013;52:585–9.

462 13. Tiwary R, Yu W, deGraffenried LA, Sanders BG, Kline K. Targeting cholesterol-rich microdomains to
463 circumvent tamoxifen-resistant breast cancer. Breast Cancer Res BCR. 2011;13:R120.

464 14. Borgquist S, Giobbie-Hurder A, Ahern TP, Garber JE, Colleoni M, Láng I, et al. Cholesterol,
465 Cholesterol-Lowering Medication Use, and Breast Cancer Outcome in the BIG 1-98 Study. J Clin Oncol
466 Off J Am Soc Clin Oncol. 2017;35:1179–88.

467 15. Kangaspeska S, Hultsch S, Jaiswal A, Edgren H, Mpindi J-P, Eldfors S, et al. Systematic drug screening
468 reveals specific vulnerabilities and co-resistance patterns in endocrine-resistant breast cancer. BMC
469 Cancer. 2016;16:378.

470 16. McBryan J, Fagan A, McCartan D, Bane FT, Varešlija D, Cocchiglia S, et al. Transcriptomic Profiling of
471 Sequential Tumors from Breast Cancer Patients Provides a Global View of Metastatic Expression
472 Changes Following Endocrine Therapy. Clin Cancer Res Off J Am Assoc Cancer Res. 2015;21:5371–9.

473 17. Subik K, Lee J-F, Baxter L, Strzepek T, Costello D, Crowley P, et al. The Expression Patterns of ER, PR,
474 HER2, CK5/6, EGFR, Ki-67 and AR by Immunohistochemical Analysis in Breast Cancer Cell Lines. Breast
475 Cancer Basic Clin Res. 2010;4:35–41.

476 18. Kumar A, Kankainen M, Parsons A, Kallioniemi O, Mattila P, Heckman CA. The impact of RNA
477 sequence library construction protocols on transcriptomic profiling of leukemia. BMC Genomics.
478 2017;18:629.

479 19. Nicorici D, Satalan M, Edgren H, Kangaspeska S, Murumagi A, Kallioniemi O, et al. FusionCatcher - a
480 tool for finding somatic fusion genes in paired-end RNA-sequencing data. bioRxiv. 2014;011650.

481 20. Barrett T, Wilhite SE, Ledoux P, Evangelista C, Kim IF, Tomashevsky M, et al. NCBI GEO: archive for
482 functional genomics data sets--update. Nucleic Acids Res. 2013;41:D991-995.

483 21. Liao Y, Smyth GK, Shi W. featureCounts: an efficient general purpose program for assigning sequence
484 reads to genomic features. Bioinforma Oxf Engl. 2014;30:923–30.

485 22. Smedley D, Haider S, Durinck S, Pandini L, Provero P, Allen J, et al. The BioMart community portal: an
486 innovative alternative to large, centralized data repositories. Nucleic Acids Res. 2015;43:W589-598.

487 23. Robinson MD, Oshlack A. A scaling normalization method for differential expression analysis of RNA-
488 seq data. Genome Biol. 2010;11:R25.

489 24. Robinson MD, McCarthy DJ, Smyth GK. edgeR: a Bioconductor package for differential expression
490 analysis of digital gene expression data. Bioinforma Oxf Engl. 2010;26:139–40.

491 25. Smyth GK, Speed T. Normalization of cDNA microarray data. Methods San Diego Calif. 2003;31:265–
492 73.

493 26. Chen EY, Tan CM, Kou Y, Duan Q, Wang Z, Meirelles GV, et al. Enrichr: interactive and collaborative
494 HTML5 gene list enrichment analysis tool. BMC Bioinformatics. 2013;14:128.

495 27. Kuleshov MV, Jones MR, Rouillard AD, Fernandez NF, Duan Q, Wang Z, et al. Enrichr: a
496 comprehensive gene set enrichment analysis web server 2016 update. Nucleic Acids Res. 2016;44:W90-
497 97.

498 28. Bligh EG, Dyer WJ. A rapid method of total lipid extraction and purification. Can J Biochem Physiol.
499 1959;37:911–7.

500 29. Schneider CA, Rasband WS, Eliceiri KW. NIH Image to ImageJ: 25 years of image analysis. Nat
501 Methods. 2012;9:671–5.

502 30. Leivonen S-K, Mäkelä R, Ostling P, Kohonen P, Haapa-Paananen S, Kleivi K, et al. Protein lysate
503 microarray analysis to identify microRNAs regulating estrogen receptor signaling in breast cancer cell
504 lines. Oncogene. 2009;28:3926–36.

505 31. Aits S, Jäättelä M, Nylandsted J. Methods for the quantification of lysosomal membrane
506 permeabilization: a hallmark of lysosomal cell death. Methods Cell Biol. 2015;126:261–85.

507 32. Pemovska T, Kontro M, Yadav B, Edgren H, Eldfors S, Szwajda A, et al. Individualized systems
508 medicine strategy to tailor treatments for patients with chemorefractory acute myeloid leukemia.
509 Cancer Discov. 2013;3:1416–29.

510 33. Yadav B, Pemovska T, Szwajda A, Kulesskiy E, Kontro M, Karjalainen R, et al. Quantitative scoring of
511 differential drug sensitivity for individually optimized anticancer therapies. Sci Rep. 2014;4:5193.

512 34. Smith K, Li Y, Piccinini F, Csucs G, Balazs C, Bevilacqua A, et al. CIDRE: an illumination-correction
513 method for optical microscopy. Nat Methods. 2015;12:404–6.

514 35. Kamentsky L, Jones TR, Fraser A, Bray M-A, Logan DJ, Madden KL, et al. Improved structure, function
515 and compatibility for CellProfiler: modular high-throughput image analysis software. Bioinforma Oxf
516 Engl. 2011;27:1179–80.

517 36. Rochefort H, Capony F, Augereau P, Cavailles V, Garcia M, Morisset M, et al. The estrogen-regulated
518 52K-cathepsin-D in breast cancer: from biology to clinical applications. Int J Rad Appl Instrum B.
519 1987;14:377–84.

520 37. Long BJ, van den Berg HW. Reduced levels of cathepsin D associated with tamoxifen resistance and
521 estrogen independence in the ZR-75-1 human breast cancer cell line. Cancer Lett. 1996;99:233–8.

522 38. Galluzzi L, Bravo-San Pedro JM, Kroemer G. Organelle-specific initiation of cell death. Nat Cell Biol.
523 2014;16:728–36.

524 39. Chan HJ, Li H, Liu Z, Yuan Y-C, Mortimer J, Chen S. SERPINA1 is a direct estrogen receptor target gene
525 and a predictor of survival in breast cancer patients. Oncotarget. 2015;6:25815–27.

526 40. Luo X, Cheng C, Tan Z, Li N, Tang M, Yang L, et al. Emerging roles of lipid metabolism in cancer
527 metastasis. Mol Cancer. 2017;16:76.

528 41. Suárez Y, Fernández C, Gómez-Coronado D, Ferruelo AJ, Dávalos A, Martínez-Botas J, et al.
529 Synergistic upregulation of low-density lipoprotein receptor activity by tamoxifen and lovastatin.
530 Cardiovasc Res. 2004;64:346–55.

531 42. Appelqvist H, Nilsson C, Garner B, Brown AJ, Kågedal K, Ollinger K. Attenuation of the lysosomal
532 death pathway by lysosomal cholesterol accumulation. Am J Pathol. 2011;178:629–39.

533 43. Fehrenbacher N, Bastholm L, Kirkegaard-Sørensen T, Rafn B, Bøttzauw T, Nielsen C, et al.
534 Sensitization to the lysosomal cell death pathway by oncogene-induced down-regulation of lysosome-
535 associated membrane proteins 1 and 2. Cancer Res. 2008;68:6623–33.

536 44. Aits S, Jäättelä M. Lysosomal cell death at a glance. J Cell Sci. 2013;126:1905–12.

537 45. Liaudet-Coopman E, Beaujouin M, Derocq D, Garcia M, Glondu-Lassis M, Laurent-Matha V, et al.
538 Cathepsin D: newly discovered functions of a long-standing aspartic protease in cancer and apoptosis.
539 Cancer Lett. 2006;237:167–79.

540 46. ClinicalTrials.gov, NCT03323346. Phase II Trial of Disulfiram With Copper in Metastatic Breast Cancer
541 - ClinicalTrials.gov [Internet]. [cited 2018 Feb 14]. Available from:
542 https://clinicaltrials.gov/ct2/show/NCT03323346

543 47. Simões BM, O'Brien CS, Eyre R, Silva A, Yu L, Sarmiento-Castro A, et al. Anti-estrogen Resistance in
544 Human Breast Tumors Is Driven by JAG1-NOTCH4-Dependent Cancer Stem Cell Activity. Cell Rep.
545 2015;12:1968–77.

546 48. Hangauer MJ, Viswanathan VS, Ryan MJ, Bole D, Eaton JK, Matov A, et al. Drug-tolerant persister
547 cancer cells are vulnerable to GPX4 inhibition. Nature. 2017;551:247–50.

548 49. Aon MA, Bhatt N, Cortassa SC. Mitochondrial and cellular mechanisms for managing lipid excess.
549 Front Physiol. 2014;5:282.

550 50. Beloribi-Djefaflia S, Vasseur S, Guillaumond F. Lipid metabolic reprogramming in cancer cells.
551 Oncogenesis. 2016;5:e189.

552 51. Qiu B, Ackerman D, Sanchez DJ, Li B, Ochocki JD, Grazioli A, et al. HIF2α-Dependent Lipid Storage
553 Promotes Endoplasmic Reticulum Homeostasis in Clear-Cell Renal Cell Carcinoma. Cancer Discov.
554 2015;5:652–67.

555 52. Zhao F, Xie P, Jiang J, Zhang L, An W, Zhan Y. The effect and mechanism of tamoxifen-induced
556 hepatocyte steatosis in vitro. Int J Mol Sci. 2014;15:4019–30.

557

558 **Figures and tables**

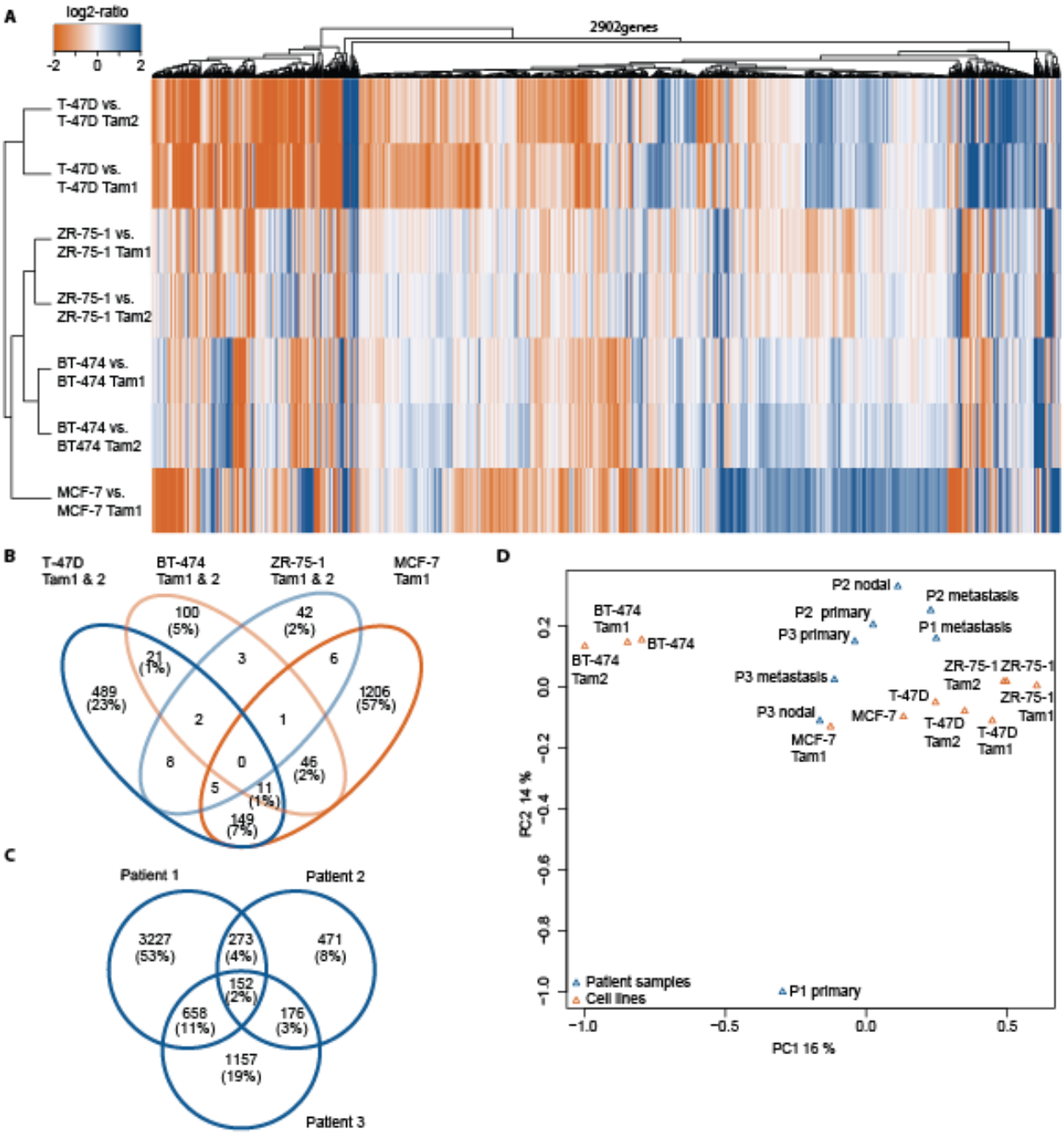

559

560 **Figure 1**: Tamoxifen-resistant cell lines display distinct expression changes and share similarities with
561 patient cases. **A** Hierarchical clustering and heat map visualization of each parental/resistant cell line pair.
562 Orange (negative log2-ratio) represents increase and blue (positive log2-ratio) decrease in expression in
563 the resistant cell lines. Only protein coding genes with log2 ratio >|1| and the difference of gene
564 expression > |10| CPM in at least one of the comparisons are displayed. Log2 ratios of >= |2| are displayed
565 in the same color. Tamoxifen-resistant clones (**B**) and patient samples (**C**) differ in their expression changes.
566 Parental is compared with resistant cell line and primary tumor with metastatic tumor from the same
567 patient, respectively. Venn diagrams show overlap in numbers and percentage of genes that are
568 differentially expressed. **D** PCA plot indicates that patients share expression patterns with the luminal A
569 cells.

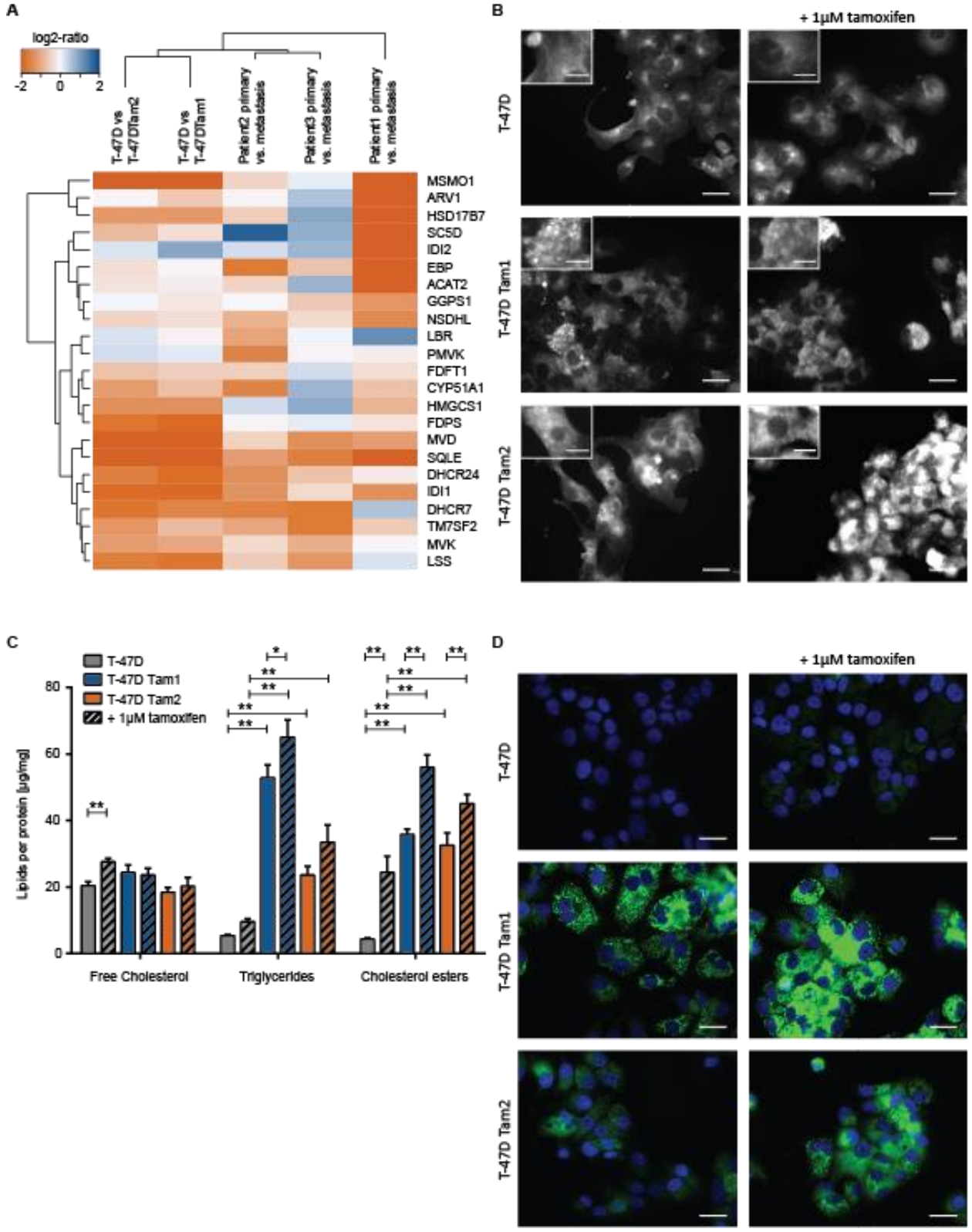

Figure 2: Genes of cholesterol pathway and related lipids are upregulated in the tamoxifen-resistant T-47D cell lines. **A** Hierarchical clustering and heat map visualization of each parental/resistant cell line pair

573 and patient primary/metastatic tumor. Orange (negative log2-ratio) represents increase and blue
574 (positive log2-ratio) decrease in expression in the resistant cell lines/metastatic tumor. Log2 ratios of >=
575 |2| are displayed in the same color. **B** Filipin staining reveals an increase in intracellular amounts of free
576 cholesterol in tamoxifen-resistant T-47D cells +/- 1µM 4-OH- tamoxifen. **C** Quantification of lipid content
577 in cells grown +/- 1µM 4-OH-tamoxifen reveals an increase in cholesterol esters and triglycerides in
578 tamoxifen-resistant cells (depicted as colored bars). Only significant differences (p-value <0.05) between
579 the same clone as well as of the comparison between resistant and tamoxifen-resistant cells in the same
580 treatment conditions are indicated all other comparisons can be found in Additional File 3. **D**
581 LipidToxGreen staining of neutral lipids (green) demonstrates that accumulation of neutral lipids into lipid
582 droplets in tamoxifen-resistant cells. The nuclei (blue) were stained with Hoechst.

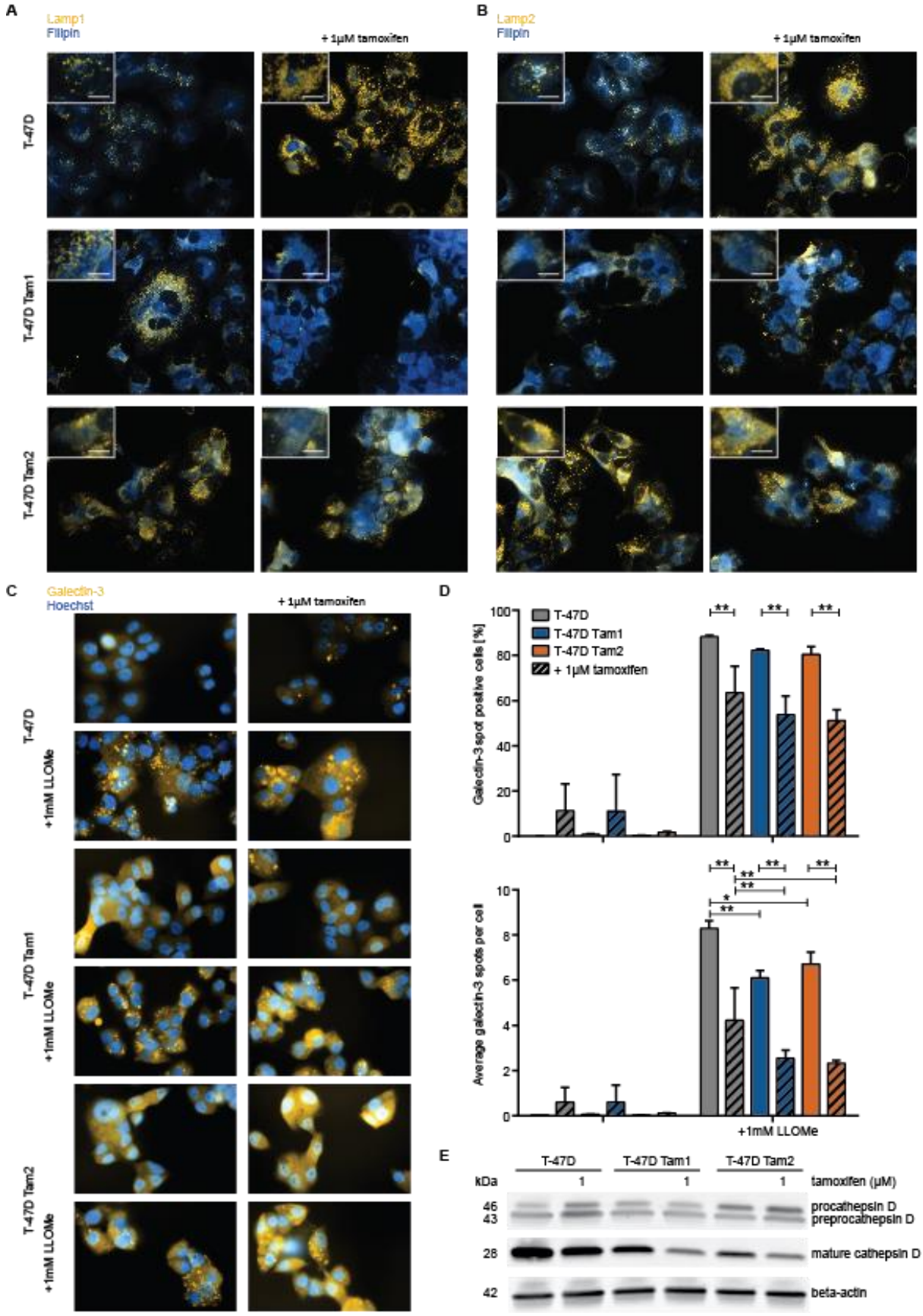
A
Lamp1
Filipin
+ 1µM tamoxifen
T-47D
T-47D Tam1
T-47D Tam2
B
Lamp2
Filipin
+ 1µM tamoxifen
C
Galectin-3
Hoechst
+ 1µM tamoxifen
T-47D
+1mM LLOMe
T-47D Tam1
+1mM LLOMe
T-47D Tam2
+1mM LLOMe
D
T-47D
T-47D Tam1
T-47D Tam2
+ 1µM tamoxifen
Galectin-3 spot positive cells [%]
Average galectin-3 spots per cell
+1mM LLOMe
E
T-47D
T-47D Tam1
T-47D Tam2
kDa
tamoxifen (µM)
46
43
procathepsin D
preprocathepsin D
28
mature cathepsin D
42
beta-actin

583

584 **Figure 3**: Free cholesterol accumulates in lysosomes in the resistant cells. Intracellular accumulation of
585 free cholesterol (blue) accumulates in lysosomes (orange) stained with two lysosomal markers, Lamp1 (**A**)
586 and Lamp2 (**B**), detecting the lysosomal-associated-membrane-proteins 1 and 2 +/- 1µM 4-OH-tamoxifen.
587 Tamoxifen-resistant cells are less sensitive to lysosomal membrane premeabilization detected with
588 galectin-3 (orange) translocation (**C**, images were differently enhanced for visualization purposes) and
589 measurement of galectin-3 positive cells (**D** upper graph) as well as number of galectin-spots per cell (**D**
590 lower image). Galectin-3 measurements were done on the raw image. Only significant differences (p-value
591 <0.05) between the same clone as well as of the comparison between resistant and tamoxifen-resistant
592 cells in the same treatment conditions are indicated all other comparisons can be found in Additional File
593 3. **E** Mature cathepsin D is downregulated in tamoxifen resistant cells.

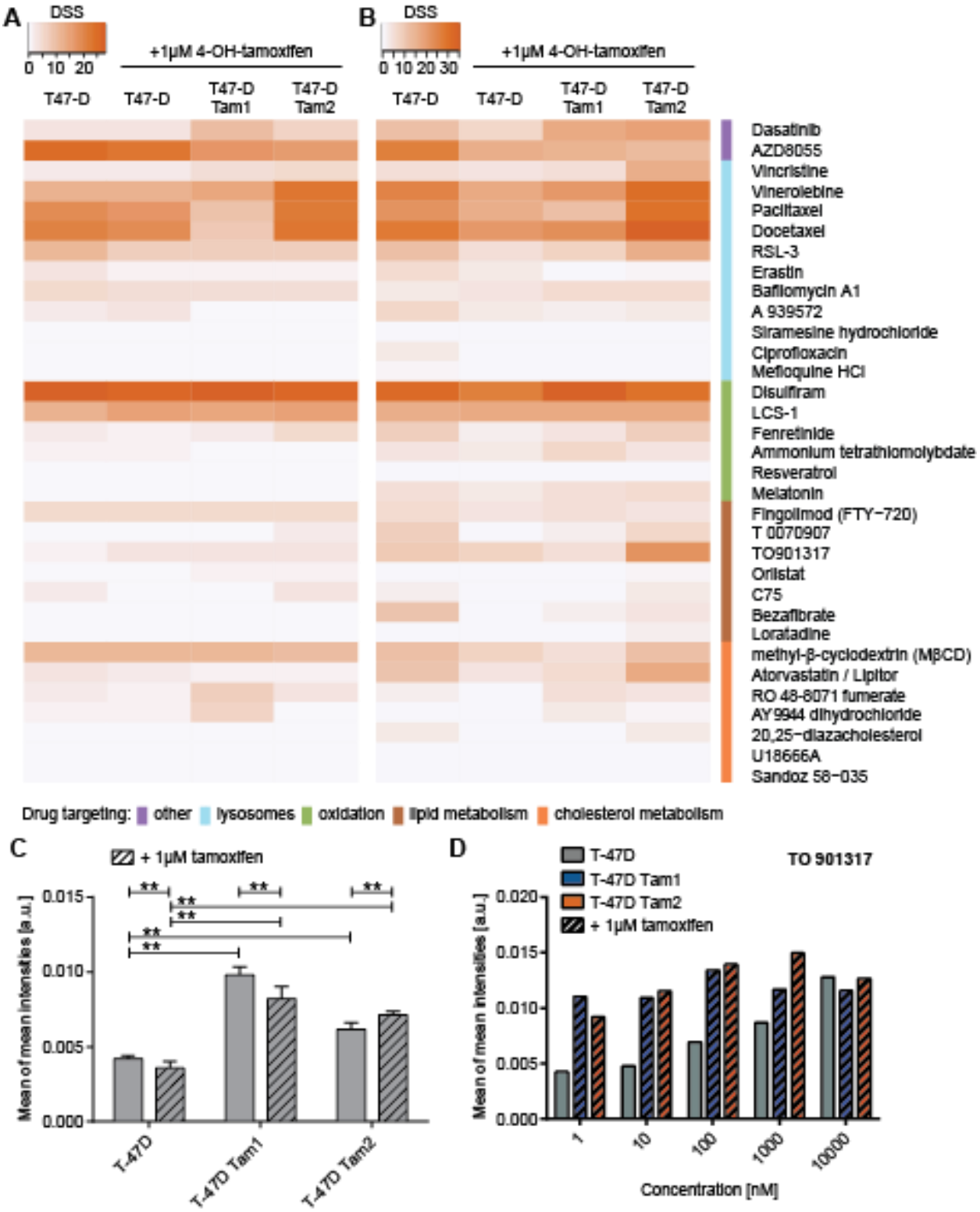

Figure 4: Drug sensitivity and resistance testing of tamoxifen resistant cells. DSS scores of **A** CTG-measurement and **B** cell count are displayed as heatmap with dark orange showing the most effective drugs. **C** Quantification of LipidToxGreen staining in cells grown +/- 1µM 4-OH-tamoxifen reveals an

598 increase in the mean intensities of the staining in tamoxifen resistant cell lines. Only significant differences
599 (p-value <0.05) between the same clone as well as of the comparison between resistant and tamoxifen-
600 resistant cells in the same treatment conditions are indicated all other comparisons can be found in
601 Additional File 3. **D** TO901317 increases the LipidToxGreen staining mainly in the parental cell lines

602 Table1: Differentially expressed genes

Number of	T-47D Tam1	T-47D Tam2	BT-474 Tam1	BT-474 Tam2	MCF-7 Tam1	ZR-75-1 Tam1	ZR-75-1 Tam2
differentially expressed genes	1425	1239	303	360	1424	193	158
upregulated genes	941	823	195	183	640	104	68
downregulated genes	484	416	108	177	784	89	90

603

604 Table2: TOP5 Pathways with adjusted p-value below 0,001 obtained from Enricher using the Reactome
605 2016 pathway. Resistant cell lines are compared with the isogenic parental control cells.

Cell line	**Term**	**Adjusted p-value**	**Overlap**
T47D Tam1	Cholesterol biosynthesis	1,49E-04	11/23
	Platelet activation, signaling and aggregation	1,49E-04	41/253
	Platelet degranulation	1,49E-04	24/105
	Activation of gene expression by SREBF (SREBP)	1,49E-04	14/42
	Response to elevated platelet cytosolic Ca2+	1,49E-04	24/110
T-47D Tam2	Cholesterol biosynthesis	1,28E-07	13/23
	Metabolism of lipids and lipoproteins	1,27E-05	78/659
	Activation of gene expression by SREBF (SREBP)	4,21E-05	14/42
	Platelet activation, signaling and aggregation	2,06E-04	37/253
	Regulation of cholesterol biosynthesis by SREBP (SREBF)	2,06E-05	15/55
MCF-7 Tam1	Cell Cycle	8,40E-13	96/566
	M Phase	1,80E-12	59/268
	Mitotic Cell Cycle	2,93E-12	82/462
	RHO GTPase Effectors	7,30E-11	54/255
	Signaling by Rho GTPases	1,27E-09	65/367
ZR-75-1 Tam1	MHC class II antigen presentation	3,45E-04	9/103
	Mitotic Cell Cycle	6,60E-04	17/462
	Resolution of Sister Chromatid Cohesion	8,75E-04	8/99
BT-474 Tam1	Axon guidance	7,60E-04	23/515
	Non-integrin membrane-ECM interactions	7,60E-04	7/42
BT-474 Tam2	Diseases of glycosylation	3,54E-06	13/88
	Diseases associated with O-glycosylation of proteins	3,68E-04	11/62
	O-linked glycosylation	1,83E-05	13/110

	Defective GALNT12 causes colorectal cancer 1 (CRCS1)	5,07E-05	6/18
	Defective GALNT3 causes familial hyperphosphatemic tumoral calcinosis (HFTC)	5,07E-05	6/18

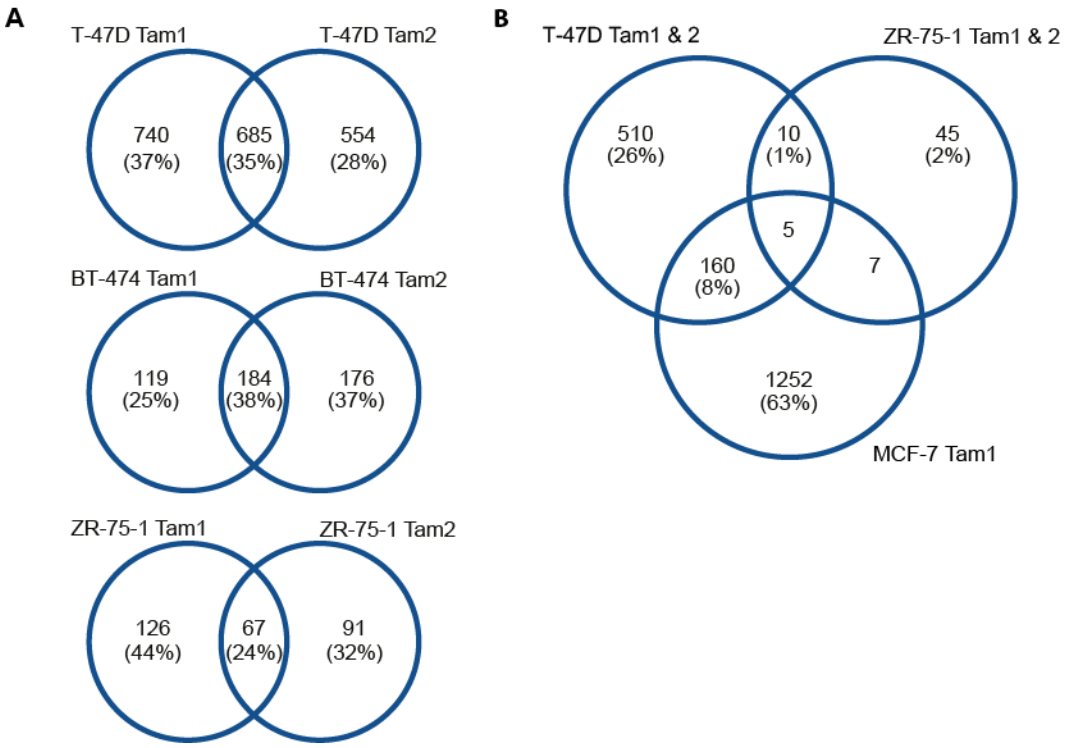

Additional figure 1 Tamoxifen-resistant cell lines display distinct expression changes. Tamoxifen-resistant clones derived from same parental cells (**A**) and of the luminal A subtype (**B**) differ in their expression changes. Venn diagrams show overlap in numbers and percentage of genes that are differentially expressed.

Additional file 1: Antibodies used in this study
Additional file 2: Drugs used in this study
Additional file 3: Statistical analysis of triglycerides, free cholesterol and cholesterol esters, LMP assay, and LipidToxGreen staining
Additional file 4: RNA-sequencing statistics
Additional file 5: Detected fusion genes of parental and tamoxifen-resistant cell lines
Additional file 6: Batch corrected CPM counts of cell lines and patients
Additional file 7: Enriched pathways with adjusted p<0.001
Additional file 8: DSS scores of CTG measurement and cell count
Additional file 9: Mean of the mean LipidToxGreen intensity values

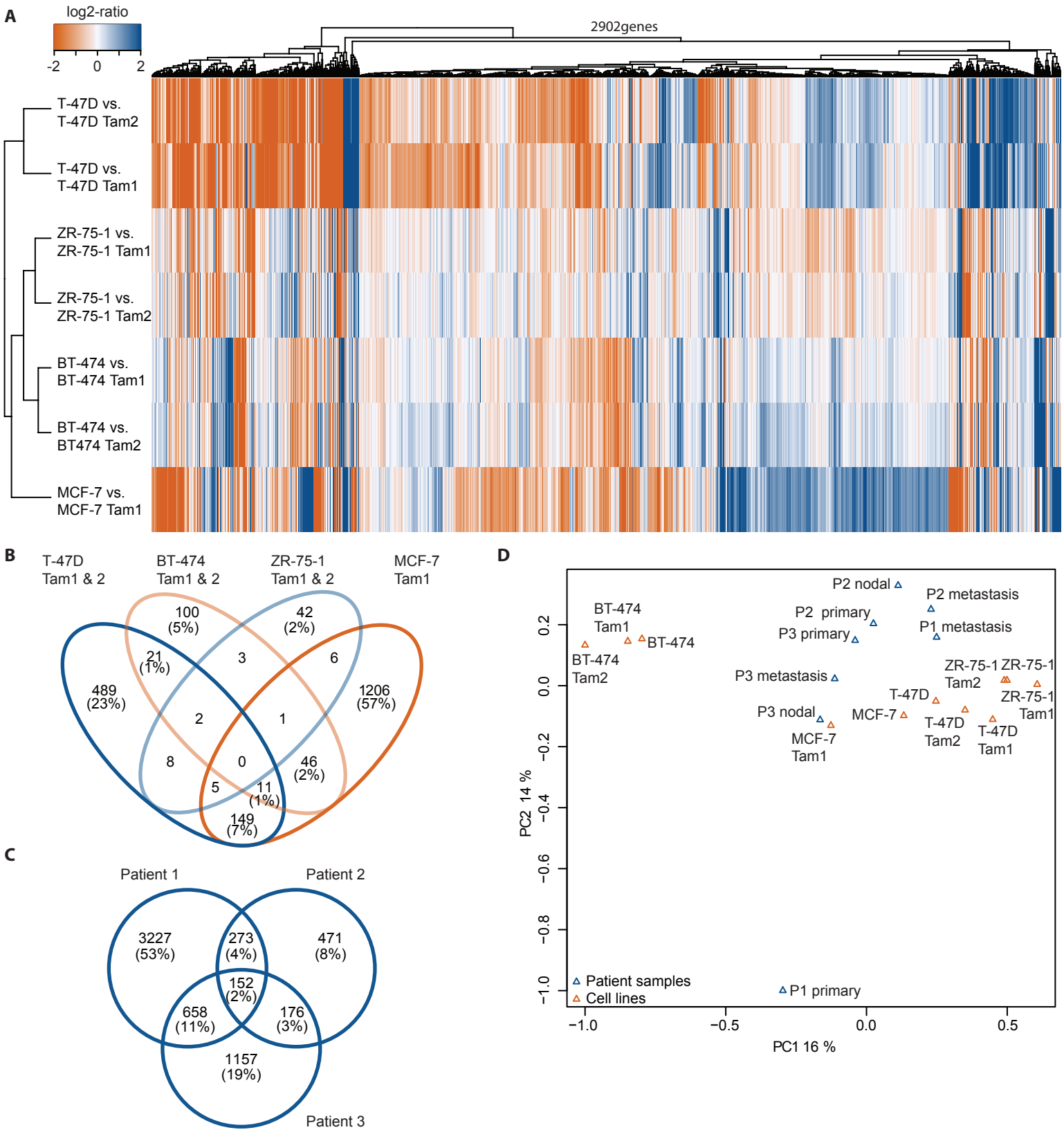
A
log2-ratio
-2
0
2
2902genes
T-47D vs.
T-47D Tam2
T-47D vs.
T-47D Tam1
ZR-75-1 vs.
ZR-75-1 Tam1
ZR-75-1 vs.
ZR-75-1 Tam2
BT-474 vs.
BT-474 Tam1
BT-474 vs.
BT474 Tam2
MCF-7 vs.
MCF-7 Tam1
B
T-47D
Tam1 & 2
BT-474
Tam1 & 2
ZR-75-1
Tam1 & 2
MCF-7
Tam1
100
(5%)
42
(2%)
21
(1%)
3
6
489
(23%)
1206
(57%)
2
1
8
0
46
(2%)
5
11
(1%)
149
(7%)
C
Patient 1
Patient 2
Patient 3
3227
(53%)
273
(4%)
471
(8%)
152
(2%)
658
(11%)
176
(3%)
1157
(19%)
D
P2 nodal
P2 metastasis
BT-474
Tam1
P2 primary
P1 metastasis
P3 primary
BT-474
BT-474
Tam2
ZR-75-1
Tam2
ZR-75-1
P3 metastasis
T-47D
ZR-75-1
Tam1
P3 nodal
MCF-7
T-47D
Tam2
T-47D
Tam1
MCF-7
Tam1
Patient samples
Cell lines
P1 primary
PC2 14 %
PC1 16 %
0.2
0.0
−0.2
−0.4
−0.6
−0.8
−1.0
−1.0
−0.5
0.0
0.5

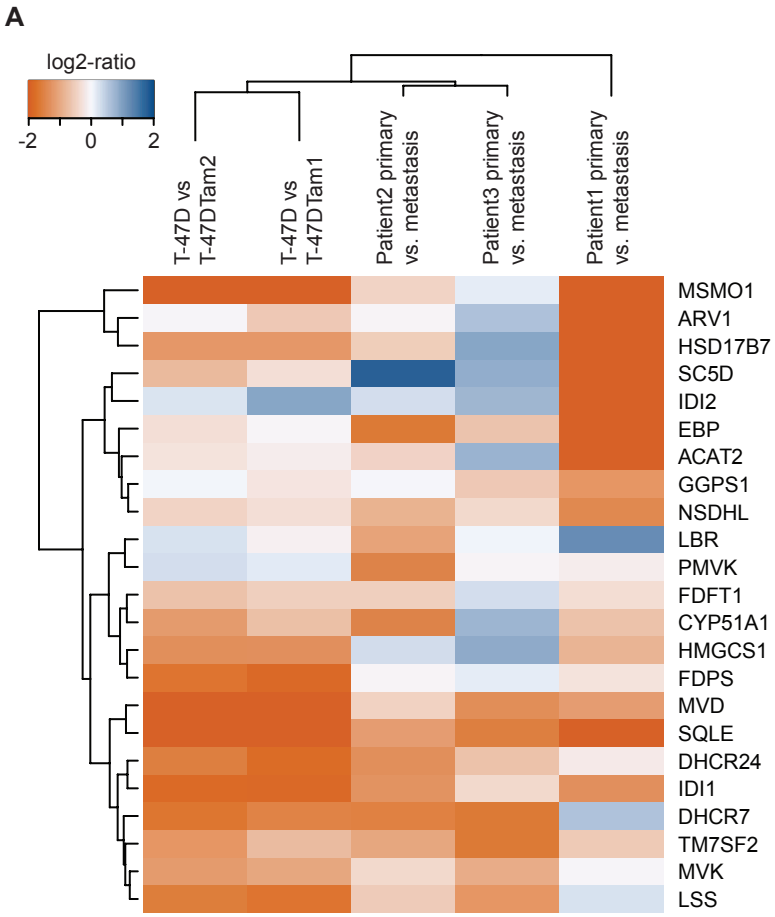
A
log2-ratio
-2
0
2
T-47D vs T-47DTam2
T-47D vs T-47DTam1
Patient2 primary vs. metastasis
Patient3 primary vs. metastasis
Patient1 primary vs. metastasis
MSMO1
ARV1
HSD17B7
SC5D
IDI2
EBP
ACAT2
GGPS1
NSDHL
LBR
PMVK
FDFT1
CYP51A1
HMGCS1
FDPS
MVD
SQLE
DHCR24
IDI1
DHCR7
TM7SF2
MVK
LSS

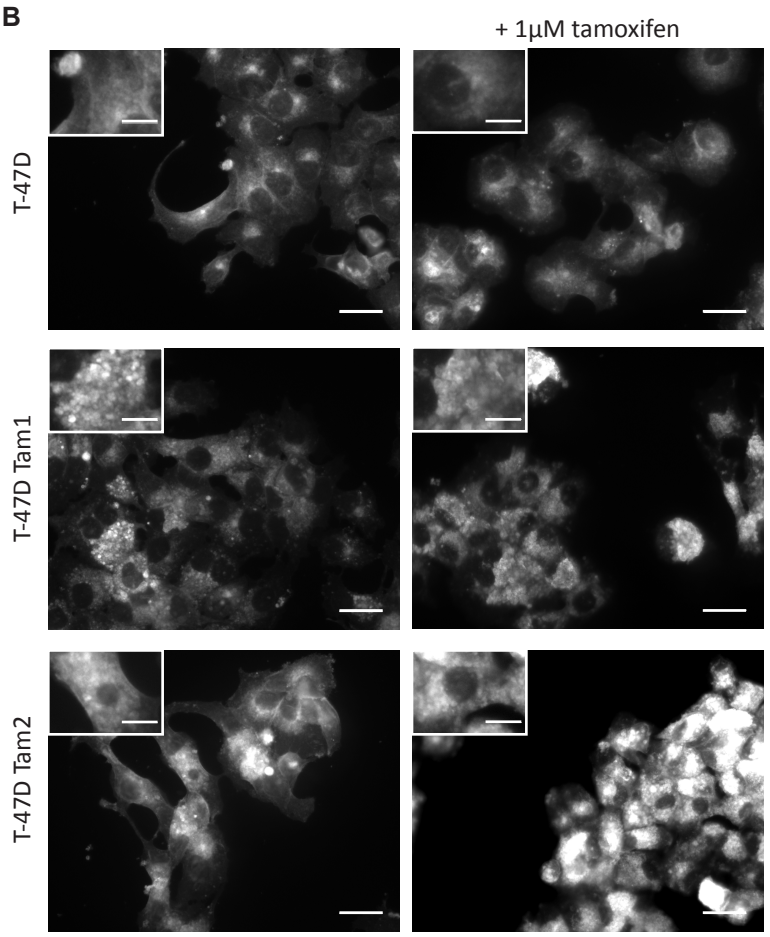
B
+ 1µM tamoxifen
T-47D
T-47D Tam1
T-47D Tam2

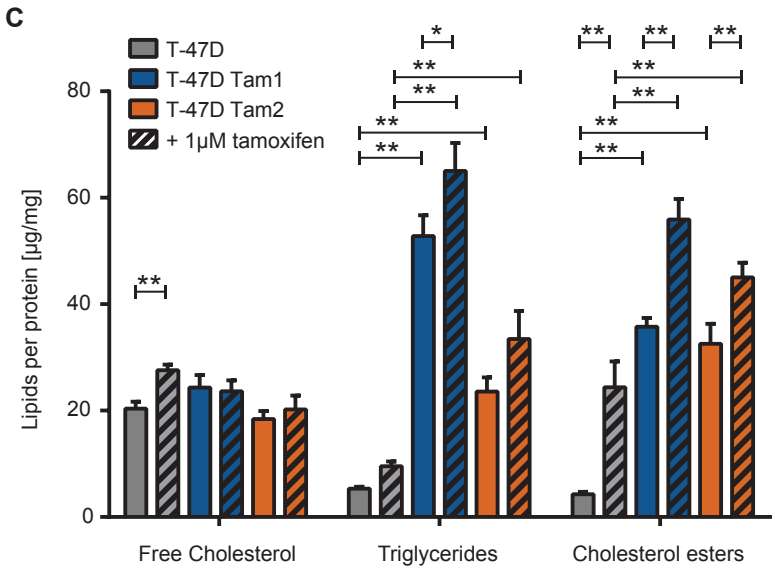
C
T-47D
T-47D Tam1
T-47D Tam2
+ 1µM tamoxifen
Lipids per protein [µg/mg]
0
20
40
60
80
Free Cholesterol
Triglycerides
Cholesterol esters

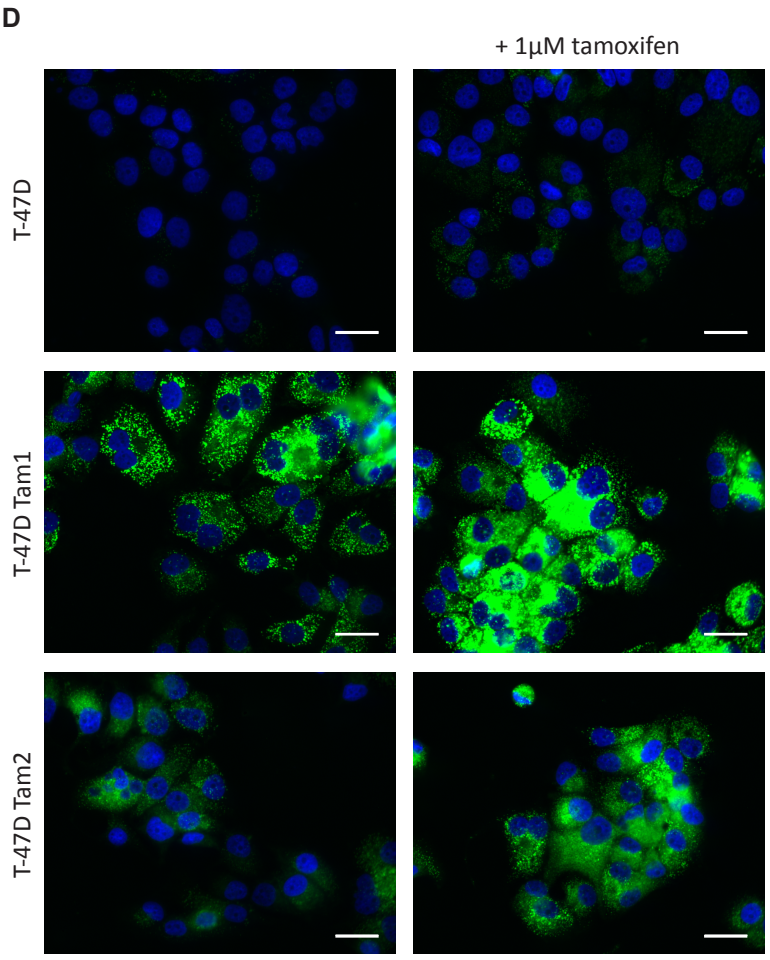
D
+ 1µM tamoxifen
T-47D
T-47D Tam1
T-47D Tam2

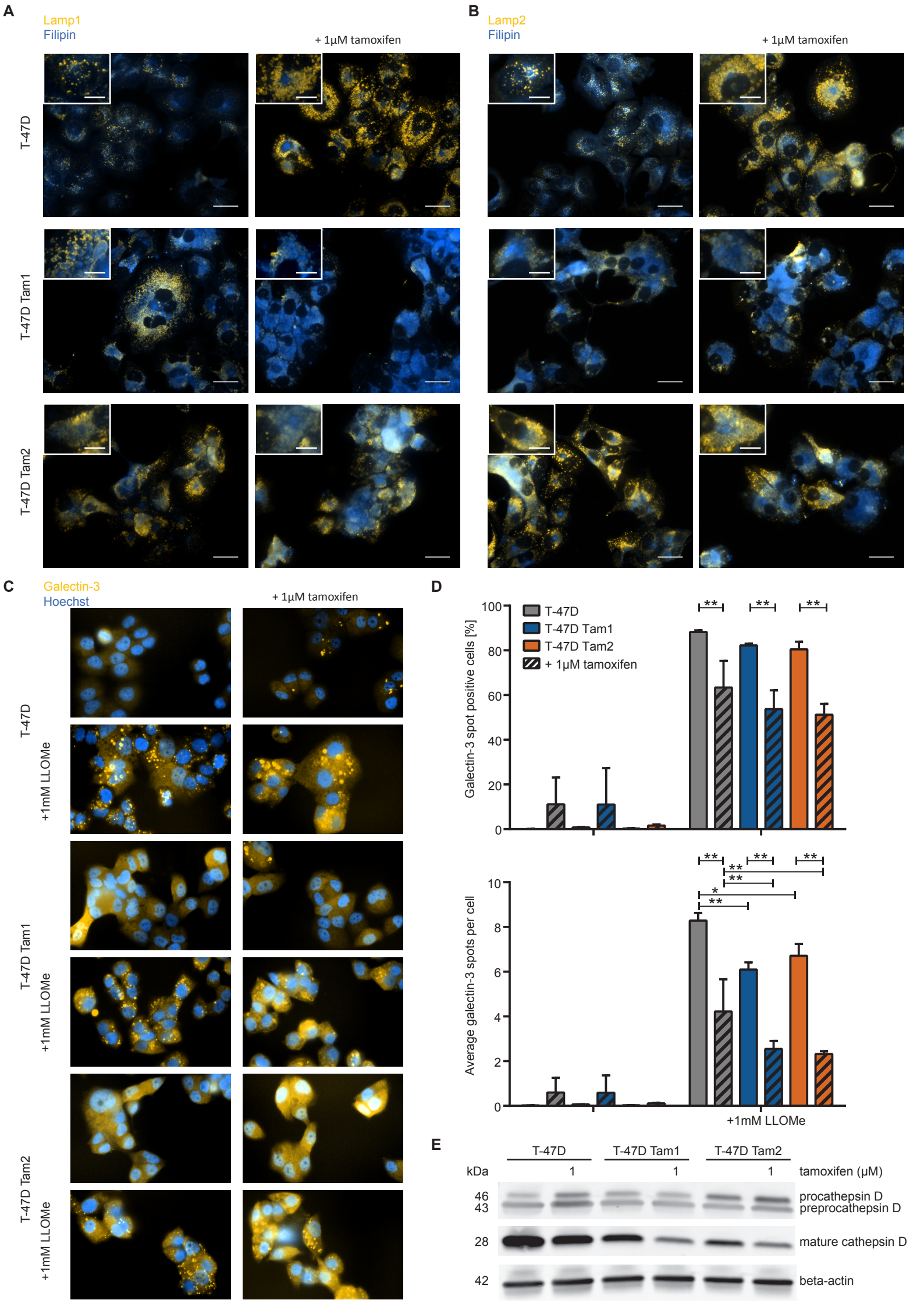
A
Lamp1
Filipin
+ 1µM tamoxifen
T-47D
T-47D Tam1
T-47D Tam2
B
Lamp2
Filipin
+ 1µM tamoxifen
C
Galectin-3
Hoechst
+ 1µM tamoxifen
T-47D
+1mM LLOMe
T-47D Tam1
+1mM LLOMe
T-47D Tam2
+1mM LLOMe
D
T-47D
T-47D Tam1
T-47D Tam2
+ 1µM tamoxifen
Galectin-3 spot positive cells [%]
Average galectin-3 spots per cell
+1mM LLOMe
E
T-47D
T-47D Tam1
T-47D Tam2
kDa
1
1
1
tamoxifen (µM)
46
43
procathepsin D
preprocathepsin D
28
mature cathepsin D
42
beta-actin

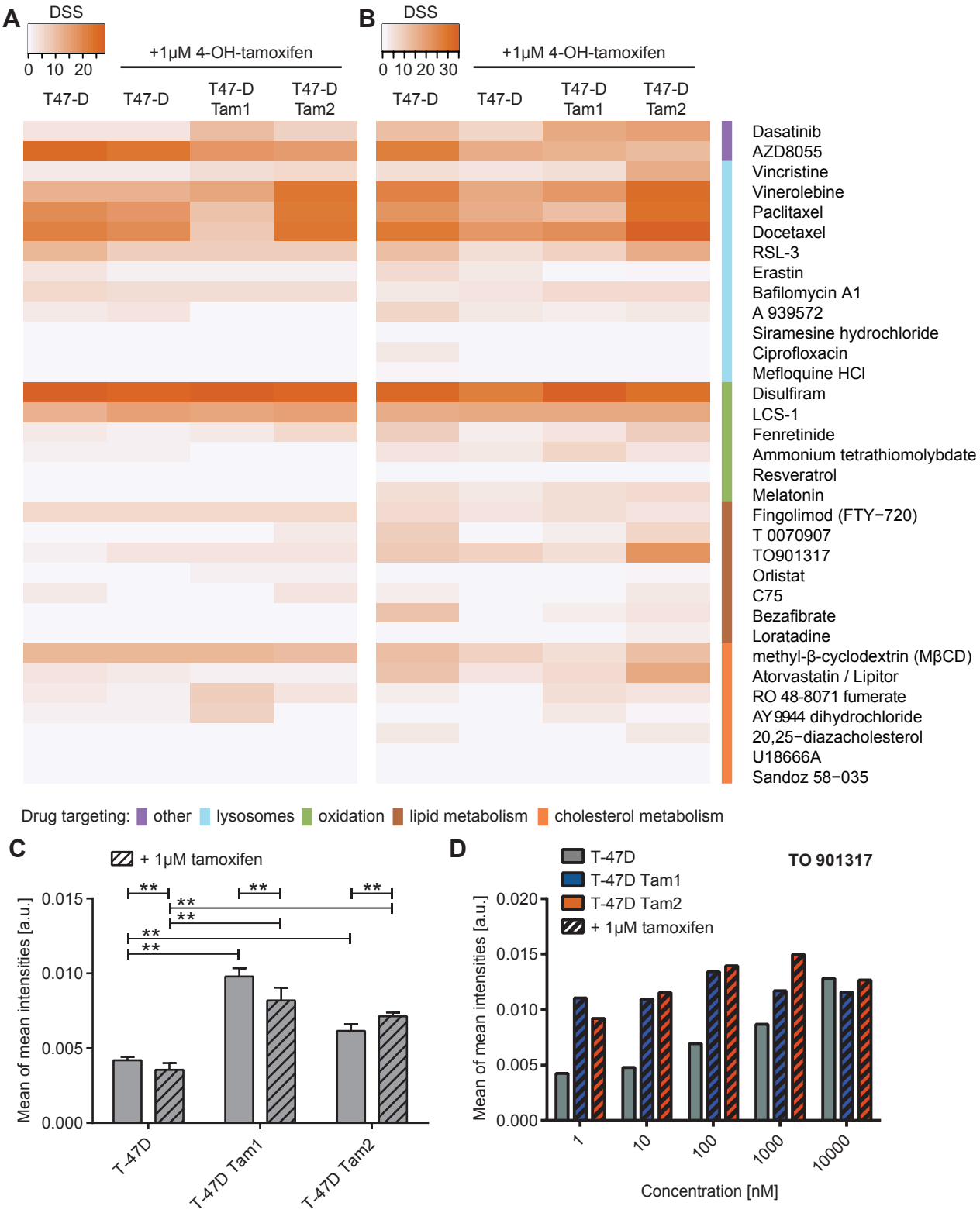
A
DSS
0 10 20
+1μM 4-OH-tamoxifen
T47-D
T47-D
T47-D Tam1
T47-D Tam2
B
DSS
0 10 20 30
+1μM 4-OH-tamoxifen
T47-D
T47-D
T47-D Tam1
T47-D Tam2
Dasatinib
AZD8055
Vincristine
Vinerolebine
Paclitaxel
Docetaxel
RSL-3
Erastin
Bafilomycin A1
A 939572
Siramesine hydrochloride
Ciprofloxacin
Mefloquine HCl
Disulfiram
LCS-1
Fenretinide
Ammonium tetrathiomolybdate
Resveratrol
Melatonin
Fingolimod (FTY−720)
T 0070907
TO901317
Orlistat
C75
Bezafibrate
Loratadine
methyl-β-cyclodextrin (MβCD)
Atorvastatin / Lipitor
RO 48-8071 fumerate
AY 9944 dihydrochloride
20,25−diazacholesterol
U18666A
Sandoz 58−035
Drug targeting: other lysosomes oxidation lipid metabolism cholesterol metabolism
C
+ 1μM tamoxifen
Mean of mean intensities [a.u.]
0.015
0.010
0.005
0.000
**
T-47D
T-47D Tam1
T-47D Tam2
D
T-47D
T-47D Tam1
T-47D Tam2
+ 1μM tamoxifen
TO 901317
Mean of mean intensities [a.u.]
0.020
0.015
0.010
0.005
0.000
1
10
100
1000
10000
Concentration [nM]